PROCEEDINGS, 46th Workshop on Geothermal Reservoir Engineering
Stanford University, Stanford, California, February 15-17, 2021
SGP-TR-218

Thermal-Hydrological-Mechanical Modeling of Stockton University Reservoir Cooling System

Torquil Smith[1], Eric Sonnenthal[1], Patrick Dobson[1], Peter Nico[1], Mark Worthington[2]

[1]Earth and Environmental Sciences Area, Lawrence Berkeley National Laboratory, 1 Cyclotron Rd., Berkeley, CA 94720

[2]Underground Energy Systems LLC., Lancaster, MA

jtsmith@lbl.gov

Keywords: THM modeling, Geothermal Cooling

ABSTRACT

Shallow aquifer water (30+ m depth) has been used for seasonal cooling of buildings at Stockton University, New Jersey, in an open loop system. High dissolved oxygen levels in a (semi-)confined aquifer led to iron hydroxide precipitation in wells after several years of operation resulting in the eventual failure and shutdown of the open loop system.

Thermal-hydrological-mechanical (THM) modeling of the system indicates some shear failure in unconsolidated sands in the aquifer in normal operation, but no failure of presumed clay layer seal of the aquifer. THM modeling of an overcapacity operation of the system results in some non-linear shearing of the clay layer seal adjacent to well bore sand pack, but no significant increase in seal layer permeability. It is not clear whether pumping at very high rates during the initial system installation phase caused breach of the clay layer seal or if seals were missing due to variation of local geologic bedding. Dissolved oxygen measured before system construction at approximately 2/3 of the atmospheric equilibrium value suggest the possibility of incomplete clay layer seals, with mixing of oxidized water from the overlying unconfined aquifer.

1. INTRODUCTION

Shallow aquifer water has been used for seasonal cooling of buildings at Stockton University, New Jersey, in an open loop system. The system includes three 'cold' wells in which chilled water is injected in winter months, and withdrawn in summer months for cooling buildings. About 300 m distant are three 'warm' wells, from which water is withdrawn for chilling in the winter months, and water warmed from cooling buildings is injected in summer months. Well locations are shown in Fig. 1.

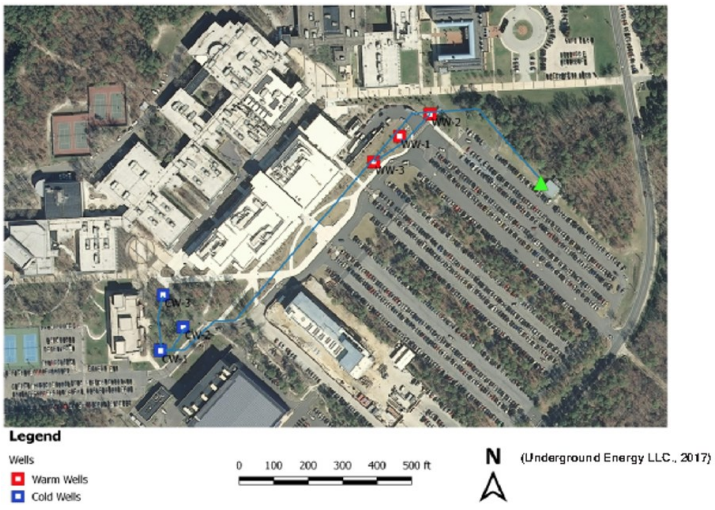

Figure 1: Location of reservoir cold storage cooling system wells at Stockton University, New Jersey.

A clay, or sand and clay, layer, separates the upper (Cohansey) sands from lower Cohansey sands at the wells, and the wells are screened in the lower Cohansey. Design specifications call for generation of 3.25×10^5 m^3 of 6˚ C water in winter, and use of 2.45×10^5 m^3 water for cooling in summer (Paksoy et al., 2009).

After some years of operation, 32-63 % injectivity was lost, with strong indications of iron hydroxide fouling (Underground Energy, 2017). Measured dissolved oxygen levels of 1.9-3.7 mg/l are high enough that microbiological iron precipitation is possible (Bauer et al., 2009) with dissolved iron at levels measured from the lower Cohansey (0.43-1.37 mg/l) (Paksoy et al., 2009; Hemphill et al., 2004; Underground Energy, 2017). Before system construction, 5.8 mg/l dissolved oxygen was measured in water from the lower Cohansey in a nearby well, but lack of fouling problems in drinking water wells with similar water composition (IF Technology and Vinokur-Pace Engin. Serv., 1997, but dissolved oxygen not assayed) in an aquifer connected up-dip (IF Technology, 2005; Sugarman, 2001) suggested that iron fouling might not be a problem.

We model the thermal, hydrological and mechanical effects of the injection and withdrawal of the cooling system waters, to check that neither system operation, nor an unscheduled initial system 'stress test' were cause of failure of the clay layer seal between the upper Cohansey sands and the lower Cohansey sands, and not thereby, a source of dissolved oxygen from the upper Cohansey waters assumed to be in rough equilibrium with atmospheric oxygen levels at the water table.

2. SYSTEM OPERATION MODEL

Based on drilling records, the clay/clay and sand layer separating the upper and lower Cohansey spans 24-30 m to 31-34 m depths. We model it as from 25.9 to 32.9 m. From records at a nearby well the lower Cohansey is underlain by the Wildwood/Belleplain (part of the Kirkwood Formation) at about 55 m depth (Sugarman, 2001), with various sedimentary units below that. We approximate units as homogenous, and either predominately clay or predominately sands, and construct a layered model shown in Fig. 2. Property ranges are given in Table 1.

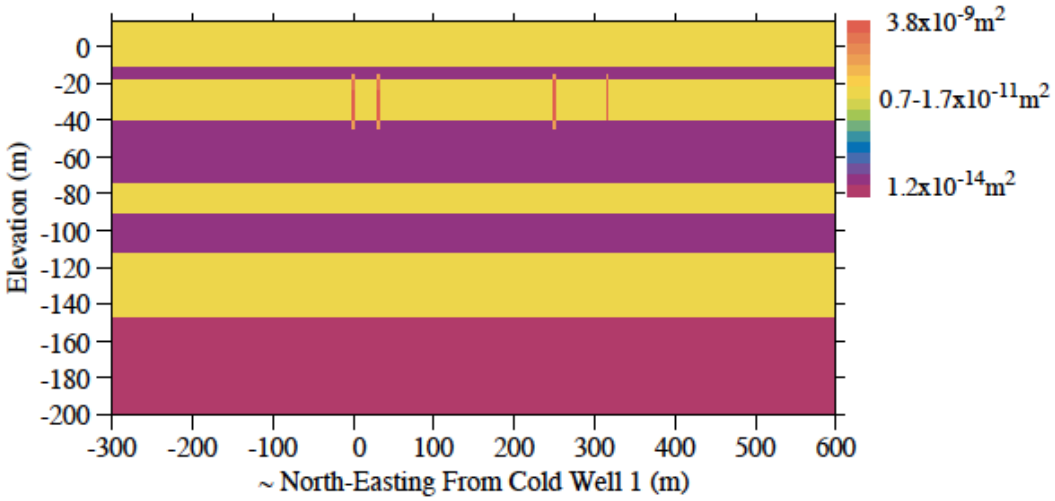

Figure 2: Cross-section of vertical permeability through cold well 1, central portion. Elements with cold wells 1 & 2 and warm wells 3 & 2 visible.

Property	Sands	Clays
porosity	0.30-0.35	0.50-0.52
horizontal permeability	$3.6\text{-}4.4\times10^{-11}$ m^2	1.0×10^{-16} -1.2×10^{-14} m^2
vertical permeability	$3.3\text{-}3.4\times10^{-11}$ m^2	1.0×10^{-16} -1.2×10^{-14} m^2
Young's modulus (drained)	15-69 MPa	160-800 MPa
shear modulus	6.9-32 MPa	73-370 MPa
Poisson ratio (drained)	0.085	0.095
friction angle	33˚	20˚
cohesion	20 kPa	41-122 kPa
tensile strength	20 kPa	0
horiz./vert. effective stress	0.5029	0.7003
Biot coefficient	0.9993-0.9998	0.7056-0.8688

Table 1: Property ranges.

Permeability of the upper clay seal (-18.9 to -11.9 m elev.) was determined from tests at a site 6 km distant. Permeability for the lower Cohansey is from pump tests at a pre-existing well on site (Mid-Atlantic Geosciences, 2004), and for other sand units and the Wildwood/Belleplain unit from Sugarman (2001) and McAuley et al. (2001). Shear moduli (small strain) for the clay layers were for kaolinite, although there are some indications of illite and smectite in clays in the Cohansey (Owens et al., 1988), at effective volumetric

(average) stress σ'_{vol} at layer depths (in elements nearest the upper clay/lower Cohansey boundary), using the parametrization of Viggiani and Atkinson (1995), assuming 20% over consolidation;

$$G = 1.964 \times 10^6 \ (\sigma'_{vol} / 1\,\text{Pa})^{0.653} \, R_{ocr}^{0.193} \tag{1}$$

where R_{ocr} is the over consolidation ratio and G is the shear modulus (in Pa).

As Cohansey sands are typically over 95% quartz, and extremely friable where exposed (and difficult to core), sands were given shear moduli for Ottawa quartz sand at similar layer depth effective volumetric stresses using the parametrization of Hardin and Richart (1963), fit to the small strain data of Richart et al. (1962).

$$G = 19000 \, \frac{(2.174 - e)^2}{1 + e} \, (\sigma'_{vol} / 1\,\text{Pa})^{1/2} \tag{2}$$

where e is void ratio $e=\phi/(1-\phi)$, and ϕ is porosity, assumed to be 0.35 in the Cohansey sands. Clay layers were given a drained condition Poisson ratio approximately consistent with data of Kawaguchi et al. (2005). Sand layers were given a drained condition Poisson ratio consistent with small strain data of Richart et al. (1962). Sand Mohr Coulomb friction angle ϕ_{fr} was fairly typical of critical state friction angles given by Bolton (1986). Critical state friction angles are generally considered to be fairly independent of confining stress (Mitchell and Soga, 2005), although there are indications of variation at very low stresses (Bishop, 1966; Rouse, 2018). The clay friction angle ϕ_{fr} is towards the low end of values for kaolinite, and a typical critical state value for montmorillonite (Mitchell and Soga, 2005). The sand cohesion represents a very lightly cemented material that crumbles easily for a shear force applied with a finger, as the Cohansey sands are highly friable. Clay tensile strength tends to be small (kPa) and measurements of it apparently decrease with increasing specimen size due to increasing numbers of internal flaws (Harison et al. 1994), so has been neglected.

The thermal, hydrological, mechanical (and chemical) modeling code Treactmech of Kim et al. (2012) was used, with modifications described in Smith et al. (2015) allowing simultaneous resolution of multiple Mohr-Coulomb failure criteria when indicated. Initial horizontal effective stresses were assumed proportional to vertical effective stresses, with proportionality constant K_0, following Kulhawy and Mayne (1990);

$$K_0 = (1 - \sin \phi_{fr}) \, R_{ocr}^{\sin \phi_{fr}} \tag{3}$$

with K_0= 0.5029 for sand layers and 0.7003 for clay layers. Modeling coordinates were aligned with cold well 1 (origin) and warm well 2. Approximately ±1 km ~SW to ~NE (x) and ~SE to ~NW (y), and 730 m vertically (z) were modelled, with 4.4 m horizontal spacing in the central 600 × 400 m in x and y, and approximately 4.5 m vertical spacing to 72 m depth, and increasing below that. The central portion is shown in Fig. 3.

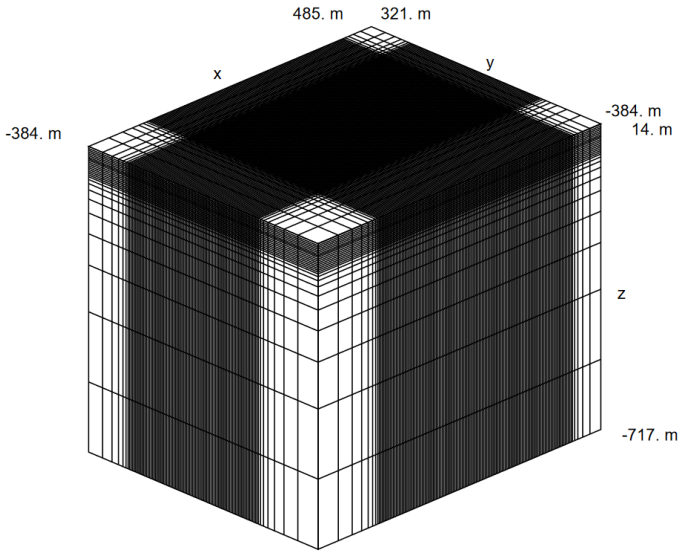

Figure 3: Central portion of area modeling grid.

An outdoor temperature of 3.9˚ C or less was estimated necessary to produce 6.1˚ C cooled water in the Stockton University cooling tower (Mid-Atlantic Geosciences, 2004). For simulation of winter flow rates, the total specified yearly cold water production was

proportioned between months with average monthly lowest temperatures below 3.9˚ C, that is, November to March (N.J. State Climatologist, 2020), approximately in proportion to their excess in heating degree days above that of the month with average lowest temperature nearest 3.9˚ C (April). Similarly, for summer flow rates, specified yearly cold water usage was divided in proportion to average monthly cooling degree days for the New Jersey coastal plain, May to October. To simulate increased cold water injection during particularly cold weather, a week of the month of January was assumed to be at system maximum pumping capacity (75.7 l/s). Simulation flow rates are plotted in Fig. 4, starting in a November.

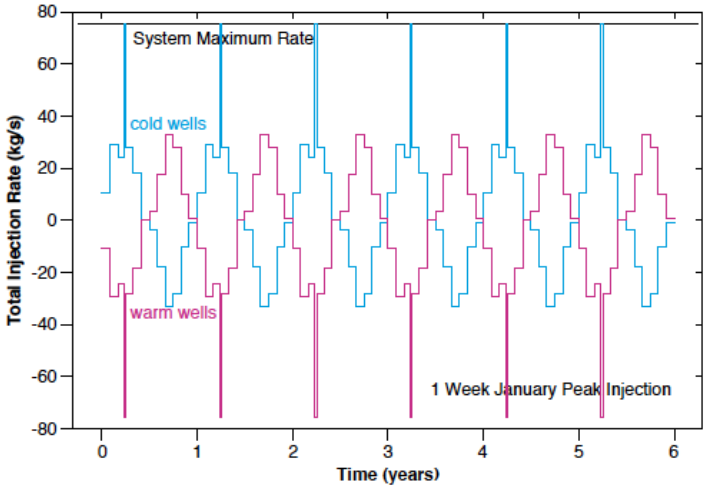

Figure 4: Simulation total injection (+) and withdrawal (-) rates for multi-year simulation.

Because more cold water is injected in winter months than is withdrawn in summer months, a volume of water near the cold water injection temperature develops and expands around the cold wells, and is shown at the end of the month of January, in the sixth year of the simulation, in Fig. 5. A smaller halo of warmed water persists around the warm wells.

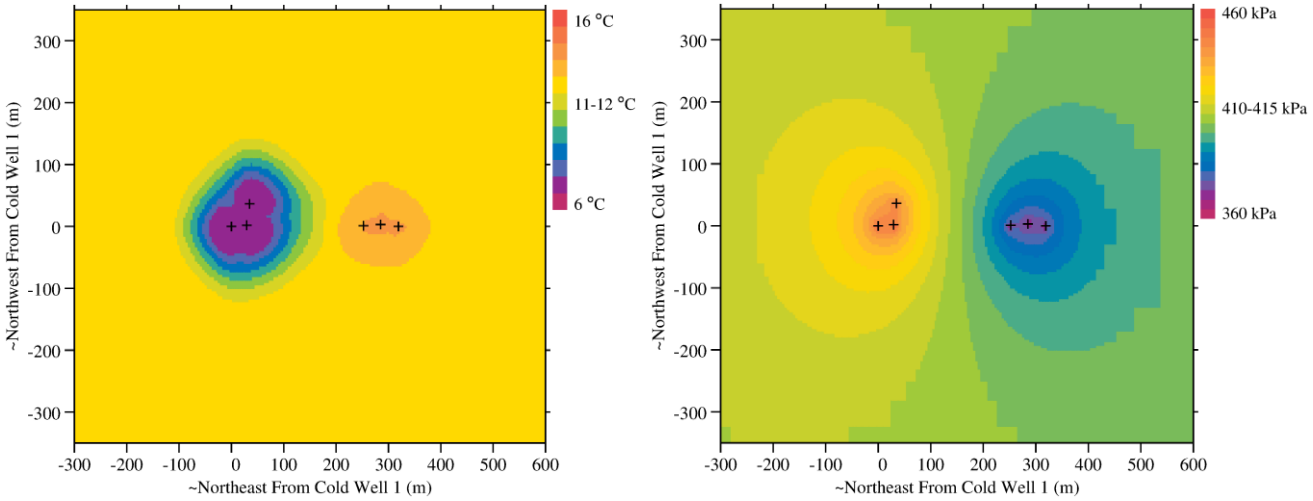

Figure 5: Temperature and fluid pressure at top of lower Cohansey, sixth year, beginning of February, plan view. Crosses at well locations.

Pressure changes from background in the lower Cohansey develop roughly in proportion to the sum of $\log(\rho_i)$ where ρ_i are the radial distances from the wells. Some failure (non-linear slip) occurs in elements with screened well in the lower Cohansey sands during peak cold water injection. Because of the element size, these elements have been given properties close to those of the lower Cohansey sands. No failure occurs in the clays in the simulation. No failure occurs in a similar simulation with January injection distributed evenly throughout the month. There no significant leakage between the upper Cohansey and lower Cohansey in these models.

3. 'STRESS TEST' SIMULATION

As previously mentioned, the system was operated at 133% of designed capacity during an initialization phase in what we refer to here as a ‘stress test’. During this, water was apparently observed at the ground surface in vicinity of cold water well 1, and the test was

discontinued after less than two hours of injection. To simulate this test, a more detailed model was made of the volume surrounding cold water well 1. To limit the domain modelled, no flow, and no normal (mechanical) displacement boundary conditions were placed at y = 18 m, and constant temperature, fluid pressure and normal stress boundary conditions were placed at x = 159 m, leaving cold wells 1 and 2 within the domain modelled for the stress test. No flow, no normal displacement boundary conditions on a bounding plane are consistent with extending the model with its reflection in the plane, as, for such a model, symmetry implies no flow nor displacement across the plane. Thus, no flow/no normal displacement boundary condition at y = 18 m has the effect of placing positive image wells at $x = x_w$, $y = 36 - y_w$, with identical injection/withdrawal as at cold wells 1 & 2, where x_w and y_w are the x and y positions of cold water well 1 or 2. Similarly, for isothermal of flow of a single fluid in a model symmetric about a plane (e.g., x=159 m), placing opposite sign fluid sources at equal distance from the symmetry plane, pairs of +/- sources cancel fluid pressure changes at the plane (to the extent that fluid density varies linearly with pressure change). And, provided there is no material failure so that stress varies linearly with strain, changes in stress components acting across the plane (e.g., σ_{xx}, σ_{xy}, σ_{xz}) cancel between pairs of fluid sources, since poroelastic porosity varies linearly with stress change. So, constant temperature/pressure/normal stress condition at x=159 m, has the effect of placing negative image wells at x= 318 - x_w, $y = y_w$. Injection at cold wells 1 & 2, corresponds to equal withdrawal at the image wells. In the non-isothermal case, the cancellation is somewhat approximate as the temperature and thus density, of water injected at one source and extracted at its reflection are not the same. The boundary conditions at x=159 m and y = 18 m also imply double (negative) image wells, reflected both in x= 159 m and in y= 36 m, for a total of two positive image wells, and four negative image wells. The boundaries at x=159 m and y = 18 m were chosen so that, approximating pressure changes in the lower Cohansey as due to vertical line sources in a confined layer, for which steady state pressure varies logarithmically with distance, at cold well 1 the sum of the pressure contributions from the two positive image (in y) and one of the negative double images, is equal to the needed contribution of cold well 3, and the sum of contributions from the two negative single images (in x), and the other double negative image, is equal to that of the three warm wells. This was gridded with horizontal spacing grading down to a 0.225×0.225 m cell for the well casing (screen) at cold well 1, and with vertical spacing down to 2 m at the clay layer between the lower and upper Cohansey. In the actual installation, one of the warm wells (1) has only 0.3 m overlap of grouted well with the clay layer, at the top of the clay layer, and below that, the well bore is sand packed outside the casing or screening. Correspondingly, the model was constructed with well grout and clay layer non-overlapping at the scale of the vertical grid (2 m). A portion of the grid in the $+x$, $+y$ corner is shown in Fig. 6.

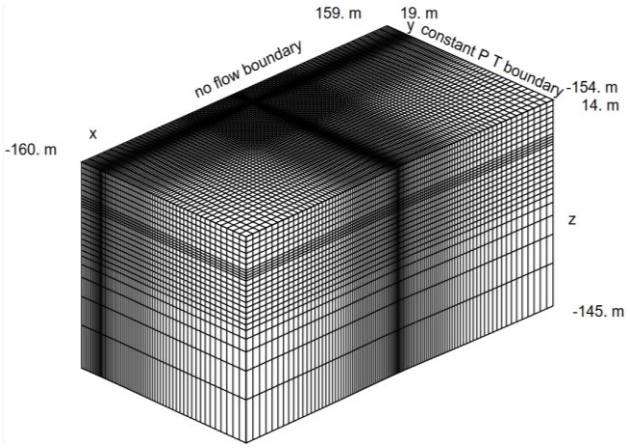

Figure 6: Part of detailed grid around cold well 1, $+x$, $+y$ corner.

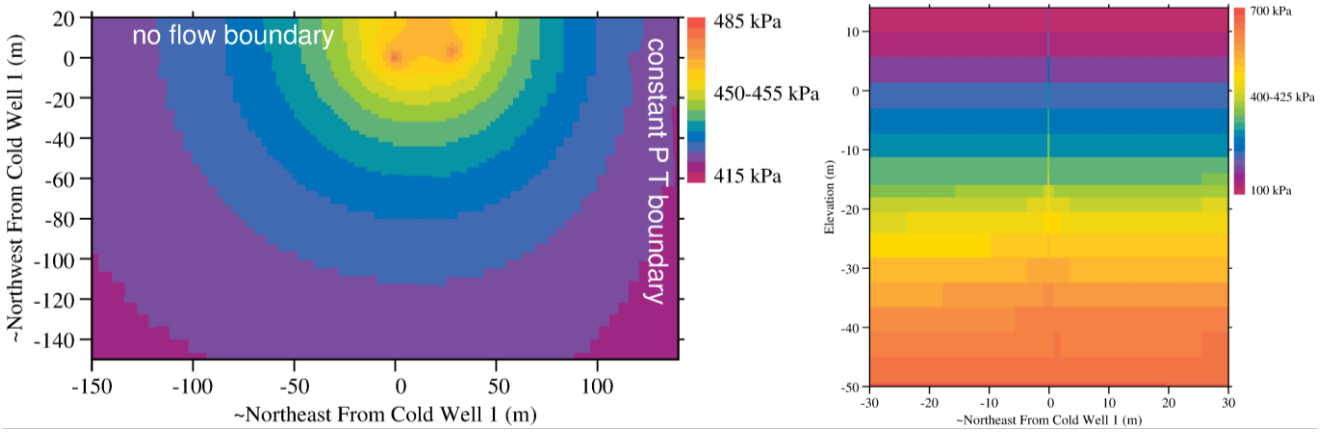

Figure 7: Fluid pressure at end of two hours injection at 101 kg/s in detailed model around cold well 1. (left) plan view at top of lower Cohansey; (right) cross section through cold well 1, detail.

Pressure at the top of the lower Cohansey at the end of two hours injection at 101 l/s total, as well as a cross-section detail through cold well 1, are shown in Fig. 7. Some material failure (non-linear shear) occurs both in the sand pack and in the clay layer adjacent to the sand pack. The non-linear strain is shown in strain `ellipsoids' at failing element centers in Fig. 8, projected in plan view, and in cross section. The figures of the ellipsoids trace the strain as a function of angle. As the strain is almost entirely shear, the ellipsoids are somewhat clover leaf in shape, with positive strain (extension) drawn in blue, and negative strain (contraction) drawn in magenta. As $+x$ and $+y$ boundaries of the modelled domain were chosen so that boundary image wells accurately reproduce at cold well 1, the pressure due to omitted wells CW 3, WW 1,2, and 3, we concentrate on the non-linear strains near cold well 1, enlarged in Fig. 9. In the elements in the clay layer outside the sand pack, non-linear strain is in extension in the azimuthal (circumferential) direction and in contraction in the vertical, and in the sand pack, primarily extensional in the radial direction and contraction in the vertical, though in the latter case principal strain axes are rotated about 30˚ from vertical and horizontal. In both cases, non-linear strain acts to diminish the difference between the vertical stress and a horizontal stress.

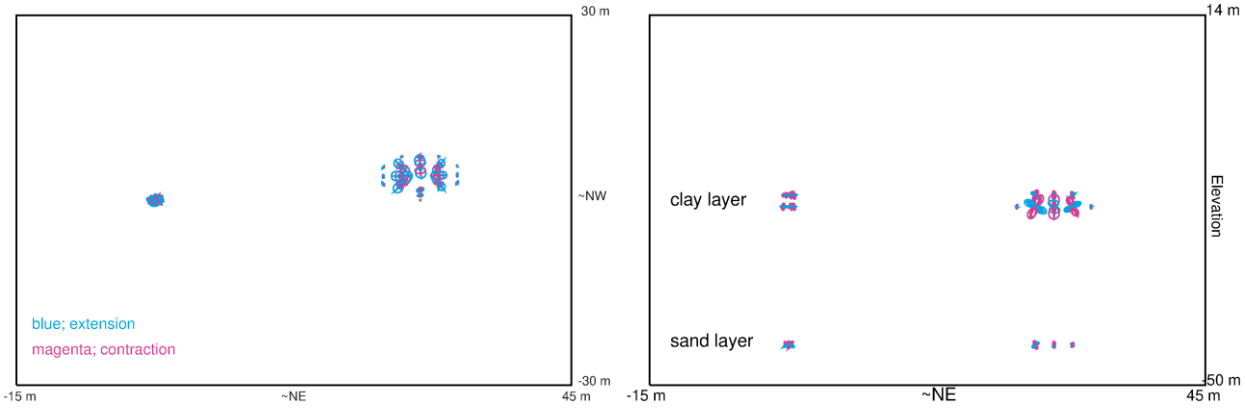

Figure 8: Non-linear (failure) strain ellipsoids, about cold wells 1 and 2; strain as a function of orientation, plotted about element centers. Projected in plan view (left) and in elevation (right).

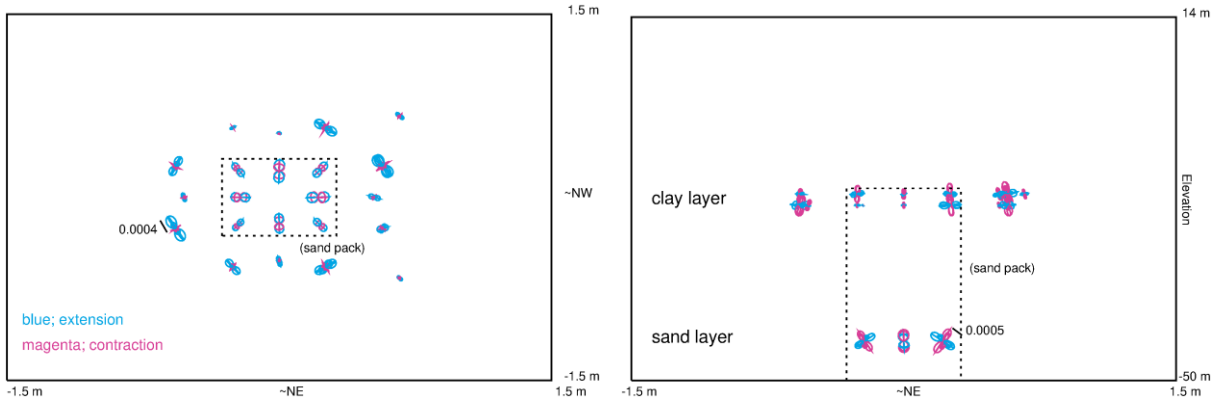

Figure 9: Non-linear (failure) strain ellipsoids, about cold well 1; strain as a function of orientation, plotted about element centers. Projected in plan view (left) and in elevation (right). Strain scale indicated. Modelled zone of sand pack around well indicated. Element centers at different y values (coordinate NW) offset slightly in elevation view.

Experimentally, clay, clay fault gouge, and clay sand mixtures appear to have reduced permeability on shearing (Lei et al. 2016; Morrow et al., 1984; Crawford et al., 2007), although in some cases may regain some permeability on further shearing (Crawford et al., 2007, at strains >1). Based on these previous studies, no increased permeability from shearing is expected, and no permeability changes on failure (non-linear slip) in the clay layer have been implemented in the current simulations. Sand approaching failure (critical state) expands (Bolton, 1986), and with that expansion (and thus increased void ratio) one expects an increase in permeability. Here, the expansion has been approximated by treating sand layers as having a 5˚ dilation angle (on failure). Sand permeability was assumed to vary as

$$k = k_0 (1-b) + k_0 b \left(1 + \Delta\phi_{fr} / (a\phi_0)\right)^3 \tag{4}$$

with a=b=10^{-6}, k_0 and ϕ_0 the initial permeability and porosity, and $\Delta\phi_{fr}$ the change in porosity due to dilation on failure. The maximum $\Delta\phi_{fr}$ was 4 x10^{-6}, so the change in permeability was negligible (8 x10^{-13} m^2) compared to the assumed sand pack permeability (3 x10^{-10} m^2). Thus, clay seals remain intact, despite injection at a rate higher than design specifications. The water pressure in cold well 1 is increased by 68 kPa above starting pressure, which corresponds to an increase of about 7 m of head. Since the water table is at roughly 5

m depth, this is enough change in head that, were there an unrestricted path to the surface, water would rise to the surface. In a simulation (not shown) with a 3 x 3 m section of the clay layer separating the upper and lower Cohansey replaced with sands about cold well 1, and a 6 x 6 m section replaced around cold well 2, pressure observed near the water table near the wells increases by 15 kPa, indicating a 1.6 m rise in water table. For a 5 m rise in water table, larger patches of clay seal would need to be sands, or there would need to be a channelized path from the well.

The three cold water wells were grouted to 30.5 m depth with neat cement without bentonite grout at the clay seal layer. It is uncertain whether they were grouted in sections or in a continuous pour (tramie). If grouted in a continuous pour, the hydrostatic stress of 1700 - 1950 kg/m^3 density grout at the bottom of a 30.5 m section exceeds hydrostatic pressure by 258-332 kPa, which is considerably greater than the estimated horizontal effective stress of 187 kPa near 30.5 m depth. In such case, it is likely that the surrounding clay fractures radially away from the grouted wells. It is not clear whether small voids might form at fracture tips and enhance vertical permeability there. This has not been modelled in the current work.

4. CONCLUSION

Simulation of operation of the Stockton University reservoir cooling system indicates that operation under the annual cycle for cooling leaves the clay seal layer separating the upper and lower Cohansey intact, and are thus not likely to be a source of upper Cohansey (more aerobic) water entering the system. Simulation of the unscheduled 'stress test' at 133 % designed capacity shows some shearing (up to 0.0004 strain) of the clay seal layer abutting well bore sand pack in the layer, but experimental results on clays, clay fault gouges and clay sand mixtures generally show permeability decrease on shearing, so this also is not a likely cause for developing a flow pathway for upper Cohansey water to enter the lower section. The apparent observation of water at the ground surface at the end of the overcapacity operation would appear to indicate at the time there was an unrestricted flow path between the well and the ground near the surface. With the well casing grouted in neat cement to 30.5 m depth with about 6.5 m overlap with a logged clay layer at the cold water wells, it is difficult to see where such a path could exist. However, Epstein and Sowers (2006) noted that well tests conducted in boreholes near the University indicated that the confining clay layer between the upper and lower Cohansey aquifers is discontinuous or leaky, which might explain the appearance of oxygenated waters over time in the lower Cohansey.

ACKNOWLEDGEMENTS

This work was supported by the U.S. Department of Energy, Office of Energy Efficiency and Renewable Energy (EERE), Office of Technology Development, Geothermal Technologies Office (GTO), under Award Number DE-AC02-05CH11231. Author J.T.S. wishes to thank K. Soga for useful references and suggestions.

REFERENCES

Bauer, M., Bendel, D., Eppinger, A., Franssen, W., Heinz, M., Keim, B., Mahler, D., Milkowski, N., Pasler, U., Rolland, K.M., Schölch-Ighodaaro, R., Stein, U., Vöröshazi, M, and Wingering, M., eds.: Arbeitshilfe zum Leitfaden zur Nutzung von Erdwärme mit Grundwasserwärmepumpe (Work aid to guideline for geothermal use of GWHP for single- and two-family houses with an energy extraction up to 45.000 kWh per year), Unweltministerium Baden-Württemberg, 0182 Stuttgart, Germany, (2009). https://um.baden-wuerttemberg.de/fileadmin/redaktion/m-um/intern/Dateien/Dokumente/5_Energie/Erneuerbare_Energien/Geothermie/4_Arbeitshilfe_zum_Leitfaden.pdf

Bishop, A.W.: Strength of soils as engineering materials, *Geotechnique*, **16**, (2), (1966), 89-130.

Bolton, M.D., The strength and dilatancy of sands, *Geotechnique*, **36**(1), (1986), 65-78.

Crawford, B.R., Faulkner, D.R., and Rutter, E.H., 2008, Strength, porosity, and permeability development during hydrostatic and shear loading of synthetic quartz-clay fault gouge, *Journal of Geophysical Research, Solid Earth*, **113**, B03207.

Epstein, C.M., and Sowers, L.S.: The continued warming of the Stockton geothermal well field, *Proceedings of ECOSTOCK 2006*, 10th International Conference on Thermal Energy Storage, The Richard Stockton College of New Jersey, Galloway, NJ, (2006).

Hardin, B.O., and Richart, Jr., F.E.: Elastic wave velocities in granular soils, *Journal of the Soil Mechanics and Foundations Division, ASCE*, **89**(SM1), (1963), 33-65.

Harison, J.A., Hardin, B.O., and Mahboub, K.: Fracture toughness of compacted cohesive soils using ring test, *Journal of Geo-technical Engineering, ASCE*, **120**, (5), (1994), 872–891.

Hemphill, B., Snijders, A., and Stiles, L.: Feasibility Study on Aquifer Thermal Energy Storage for the Richard Stockton College of New Jersey, appendix to, Mid-Atlantic Geosciences, lLC, 2004, Hydrogeologic Technical Report for Aquifer Thermal Energy Storage at Richard Stockton College of New Jersey, Atlantic County New Jersey, Mid-Atlantic Geosciences, LLC, Hammonton, New Jersey 08037, (2004).

IF Technology bv, and Vinokur-Pace Engineering Services Inc.: Feasibility Study on Aquifer Cold Storage for West Quad, Recreation Center and the Performing Arts Center at the Richard Stockton College of New Jersey, IF Technology bv, NL 6800 AP Arnhem, Netherlands, (1997).

IF Technology bv: Aquifer Thermal Energy Storage System, Richard Stockton College, New Jersey, Detailed Design ATES system, July 2005 draft, IF Technology bv, NL 6800 AP Arnhem, Netherlands, (2005).

Kawaguchi, T., Mitachi, T., and Shibuya, S.: Drained and undrained elastic moduli of reconstituted clay, *Proceedings of the 16th International Conference on Soil Mechanics and Geotechnical Engineering*, Osaka, Japan, (2005).

Kim, J., Sonnenthal, E.L., and Rutqvist, J.: Formulation and sequential numerical algorithms of coupled fluid/heat flow and geomechanics for multiple porosity materials, *Int. J. Numer. Meth. Engng.*, **92**, (2012), 425-456.

Kulhawy, F.H., and Mayne, P.W.: Manual on estimating soil properties for foundation design, Electric Power Research Institute Technical Report EPRI-EL-6800, (1990).

Lei, H., Wu, Y., Yu, Y., Zhang, B., and Lv, H.: Influence of shear on permeability of clayey soil, *International Journal of Geomechanics*, **16**(5), (2016), 04016010-1-8.

McAuley, S.D., Barringer, J.L., Paulachok, G.N., Clark, J.S., and Zapecza, O.S.: Ground-waterflow and Quality in the Atlantic City 800-foot Sand, New Jersey, New Jersey Geological Survey Geological Survey Report GSR 41, New Jersey Department of Environmental Protection, Trenton, New Jersey, (2001).

Mid-Atlantic Geosciences, LLC: Hydrogeologic Technical Report for Aquifer Thermal Energy Storage at Richard Stockton College of New Jersey, Atlantic County New Jersey, Mid-Atlantic Geosciences, LLC, Hammonton, New Jersey 08037, (2004).

Mitchell, J.K., and Soga, K.: Fundamentals of Soil Behavior, 3rd ed., John Wiley & Sons, Hoboken, New Jersey, (2005).

Morrow, C.W., Shi, L.Q., Byerlee, J.D., Permeability of fault gouge under confining pressure and shear stress, *Journal of Geophysical Research*, **89**(B5), (1984), 3193-3200.

New Jersey State Climatologist, Rutgers University, Monthly Climate Tables, https://climate.rutgers.edu/stateclim_v1/nclimdiv/index.php?stn=NJ02&elem=hdd, (2020), accessed 6/20/2020.

Owens, J.P., Bybell, L.M., Paulachok, G., Acer, T.A., and Gonzalez, V.M.: Stratigraphy of the Tertiary Sediments in a 945-Foot-Deep Corehole near Mays Landing in the Southeastern New Jersey Coastal Plain. U.S. Geological Survey Professional Paper 1484, (1988).

Paksoy, H., Snijders, A., and Stiles, L.: Aquifer thermal energy cold storage system at Richard Stockton College, *Proceedings of EFFSTOCK 2009*, Stockholm, (2009).

Richart, F.E., Hall, J.R., and Lysmer, J.: Study of the Propagation and Dissipation of "Elastic" Wave Energy in Granular Soils, report for Waterways Experimental Station, U.S. Army Corps of Engineers. Department of Civil Engineering, Industry and Engineering and Industry Experimental Station, University of Florida, (1962). https://apps.dtic.mil/dtic/tr/fulltext/u2/286075.pdf

Rouse, P.C.: Relation between the critical state friction angle of sands and low vertical stresses in the direct shear test, *Soils and Foundations*, **87**, (2018), 1282-1287.

Smith, J.T., Sonnenthal, E.L., and Cladouhos, T.: Thermal-Hydrological-Mechanical Modelling of Shear Stimulation at Newberry Volcano, Oregon. *Proceedings of 49th US Rock Mechanics/Geomechanics Symposium*, American Rock Mechanics Association, ARMA 15-0680, (2015).

Sugarman, P.J.: Hydrostratigraphy of the Kirkwood and Cohansey Formations of Miocene Age in Atlantic County and Vicinity, New Jersey, New Jersey Geological Survey Geological Survey Report GSR 40, New Jersey Department of Environmental Protection, Trenton, New Jersey, (2001).

Underground Energy, LLC.: Final Report, Aquifer Thermal Energy Storage (ATES) System Evaluation, Stockton University, Galloway, New Jersey, Underground Energy Systems, Lancaster, Mass. (2017).

Viggiani, G., and Atkinson, J.H.: Stiffness of fine-grained soil at very small strains, *Geotechnique*, **45**(2), (1995), 249-265.